The International Journal of Advanced Manufacturing Technology (2020) 109:771–779
https://doi.org/10.1007/s00170-020-05706-y

ORIGINAL ARTICLE

Investigation of load direction on the compressive strength of additively manufactured triply periodic minimal surface scaffolds

D. A. de Aquino[1] · I. Maskery[2] · G. A. Longhitano[3,4,5] · A. L. Jardini[3,4] · E. G. del Conte[1]

Received: 22 March 2020 / Accepted: 30 June 2020 / Published online: 8 July 2020

Abstract
Triply periodic minimal surfaces (TPMS) enable the construction of lightweight scaffolds, complex geometry heat exchangers, and energy absorbing materials. Additive manufacturing (AM) has the potential to build such TPMS structures due to its inherent manufacturing freedom and layer-by-layer construction; however, the manufacturing orientation in AM is known to have a significant effect on the resulting mechanical properties. The main contribution of this research is the examination of the effect of manufacturing orientation and TPMS type on the mechanical properties of scaffolds manufactured by fused deposition modeling (FDM), a widely used form of AM. The combination of compressive load direction (0° and 90° with respect to the manufacturing orientation) and TPMS type resulted in large changes in compressive strength. The primitive scaffold achieved the best performance in compression tests. It also had the shortest manufacturing time and smallest quantity of support material needed for FDM manufacture. The TPMS scaffold type combined with the loading direction significantly affected the compressive strength and elastic modulus of the scaffolds, showing the importance of considering both these properties in the design of AM scaffold structures.

Keywords Triply periodic minimal surfaces · Load direction · Compressive strength · Additive manufacturing · Fused deposition modeling

1 Introduction

Additive manufacturing's (AM) ability to produce complex geometries directly from CAD models [1] makes it an ideal choice for the study of scaffold structures. Triply periodic minimal surfaces (TPMS) can be used to generate a new range of scaffolds. These geometries present a minimal surface area, with zero-mean curvature at all points. Among these, the TPMS are characterized by a cubic symmetry and have interconnected internal void regions [1, 2].

The range of TPMS suitable for AM scaffold design is large. Several TPMS types which have received recent experimental and theoretical attention are the gyroid, primitive, and diamond surfaces; these are described by equations 1, 2, and 3, respectively [3]:

$$U_G = \cos(k_x x)\sin(k_y y) + \cos(k_y y)\sin(k_z z) + \cos(k_z z)\sin(k_x x) - t, \quad (1)$$

$$U_p = \cos(k_x x) + \cos(k_y y) + \cos(k_z z) - t, \quad (2)$$

$$U_D = \sin(k_x x)\sin(k_y y)\sin(k_z z) + \sin(k_x x)\cos(k_y y)\cos(k_z z) + \cos(k_x x)\sin(k_y y)\cos(k_z z) + \cos(k_x x)\cos(k_y y)\sin(k_z z) - t, \quad (3)$$

where the $U = 0$ isosurface represents the solid-void boundary of the scaffold and t is used to control the volume fraction of the resulting lattice. k_i is the TPMS function periodicities, defined as

✉ E. G. del Conte
erik.conte@ufabc.edu.br

[1] Federal University of the ABC, Av. dos Estados, 5001, Santo André, SP 09210-580, Brazil

[2] Centre for Additive Manufacturing, Faculty of Engineering, University of Nottingham, Nottingham NG8 1BB, UK

[3] School of Chemical Engineering, University of Campinas, Campinas, Brazil

[4] National Institute of Biofabrication (INCT-BIOFABRIS), Campinas, Brazil

[5] Center for Information Technology Renato Archer (CTI), Campinas, Brazil

Table 1 TPMS parameters

Parameter	Data
Geometry	Cubic
Dimensions	30 × 30 × 30 mm
Number of cells	3 × 3 × 3
Scaffold type	Primitive, gyroid, or diamond
Volume fraction	0.3

$$k_i = 2\pi\frac{n_i}{L_i} \text{ (with } i = x, y, z), \tag{4}$$

where n_i are the cell repetitions in the x, y, and z directions and L_i are the absolute sizes of the structure in those directions.

Scaffolds based on the TPMS equations above feature high surface-to-volume ratio and tailorable volume fraction through manipulation of the t parameter. These characteristics are beneficial for lightweight scaffolds, where the designer can specify the volume fraction and therefore stiffness of the structure, and also for high performance heat exchangers, where the high surface area contributes to increased heat transport between the solid structure and a surrounding fluid [3, 4].

Various recent works have explored TPMS manufacturing and properties. A study of the primitive TPMS scaffold made by AM showed the relevance of regular geometries without discontinuities [5]. The same work analyzed the elastic properties and yield stress of different stress states of the structure using the finite element method. In another work, the manufacturing orientation was found to have a large impact on the stiffness, strength, manufacturing time, and density of acrylonitrile butadiene styrene (ABS) parts produced by fused deposition modeling (FDM) [6]. Abueidda et al. [7] studied three types of TPMS scaffold, those based on the primitive, IWP, and neovius surface equations. The results showed good accordance between compression tests and finite element method simulations. Furthermore, the neovius and IWP scaffolds presented superior stiffness and mechanical strength compared to the primitive scaffold. Other research analyzed the energy absorbed during shock loads from four types of TPMS made of polylactic acid (PLA): gyroid, diamond, neovius, and D-prime [8]. It was found that the AM TPMS structures absorb more energy than traditional honeycombs. Maskery et al. [3] worked on the mechanical property analysis of triply periodic minimal surface with diamond, primitive, and gyroid scaffolds made from selectively laser-sintered nylon. In that work, the TPMS type and volume fraction were found to determine the mechanical properties of the scaffolds. Zhang et al. [9] investigated the mechanical properties of three TPMS sheet structures (primitive, diamond, and gyroid) manufactured by selective laser melting of 316L stainless steel and found that the unit cell geometry strongly affects the mechanical properties. Finally, in a study contributing to tissue engineering with the use of ceramic structures, Restrepo et al. [10] compared the mechanical characteristics of the diamond, primitive, and gyroid scaffolds as bone growth templates using ceramic paste.

The studies introduced above focus on mechanical properties but do not consider the effect of load direction. One of the drawbacks of AM is the anisotropic properties of manufactured parts, due to its layer-by-layer manufacturing process. Therefore, the direction of the applied load with respect to the manufacturing orientation has an important impact on the mechanical properties of AM parts [11].

This work investigates the effect of the loading direction combined with TPMS scaffold type on the compressive strength of scaffolds made by FDM. A full factorial design of experiments (DOE) was used to investigate the effect of control variables (scaffold types: primitive, gyroid, and diamond and load direction 0° and 90°) in the response variables (maximum stress and modulus of elasticity) of the scaffolds.

2 Materials and methods

Three types of TPMS scaffold were produced: primitive, gyroid, and diamond. These were chosen due to previous works that had compared the mechanical properties of the same types of TPMS [3, 9]. Their highly specific mechanical properties, tailorable geometry (and stiffness, strength, etc.) through the surface equations, and high surface-to-volume ratio make them well suited to applications including thermal management and medical implants. The parameters used for designing the samples are shown in Table 1. The scaffold

Table 2 Mechanical properties of ABS plus (Stratasy [16])

Mechanical properties	Test method	Value (XZ axis)
Tensile strength, final (type 1, 0.125″, 0.2″/min)	ASTM D638	33 MPa
Tensile strength, flow (type 1, 0.125″, 0.2″/min)	ASTM D638	31 MPa
Modulus of elasticity (type 1, 0.125″, 0.2″/min)	ASTM D638	2200 MPa
Tensile elongation at break (type 1, 0.125″, 0.2″/min)	ASTM D638	6%
Tensile elongation at stress (type 1, 0.125″, 0.2″/min)	ASTM D638	2%
IZOD Impact, groove (method A, 23 °C)	ASTM D256	106 J/m

Table 3 FDM production parameters

Material	ABS plus
Volume fraction	0.30
Layer resolution (mm)	0.25
Chamber temperature (°C)	70
Dimension (mm)	30 × 30 × 30
Model interior type	Solid
Support filling	Basic
STL scale	1.00

types and design parameters were selected considering related previous works on AM TPMS structures [3, 9].

The specimens were produced using a uPrint SE FDM printer, from commercial ABS plus filament from Stratasys. ABS was the material of choice because it is widely used in engineering applications thanks to its low cost, high toughness, and rigidity [12]. Also, ABS was the primary material that was introduced with FDM process [13] and has been found to offer greater manufacturing consistency and is more robust to processing conditions compared to PLA [14]. Finally, ABS parts produced by FDM can be modified to be hydrophilic, water-impermeable, and biocompatible without significant loss of mechanical properties and without increasing the cost of the material [15]. The material mechanical properties are given in Table 2.

CatalystEX 4.4 software was used for manufacturing planning and to measure the amount of support material and manufacturing time of the TPMS scaffold specimens. Table 3 shows the manufacturing parameters. The support material was removed with soluble support technology, which dissolves the support in a water-based solution. Figure 1 illustrates the CAD and manufactured scaffold specimens.

The compression tests on the scaffold specimens were performed with an Instron 3369 machine based on ASTM D695-15 [17]. The tests were done at room temperature with a head speed of 1.3 mm/min and total distance traveled by the loading head = 18 mm. Specimens were tested in triplicate at 0° and at 90° rotation around the *x*-axis. The stress was determined considering the effective cross-sectional area (solid area) of the specimens, which were measured with the ImageJ software and the values are primitive = 587.2 mm^2, gyroid = 687.4 mm^2, and diamond = 830.7 mm^2. Considering the two factors (scaffold type and load direction) and respective levels (primitive, gyroid, and diamond and 0° and 90°) with three replications, the full factorial DOE results in 18 experiments. Analysis of variance (ANOVA) was carried out on the experimental results.

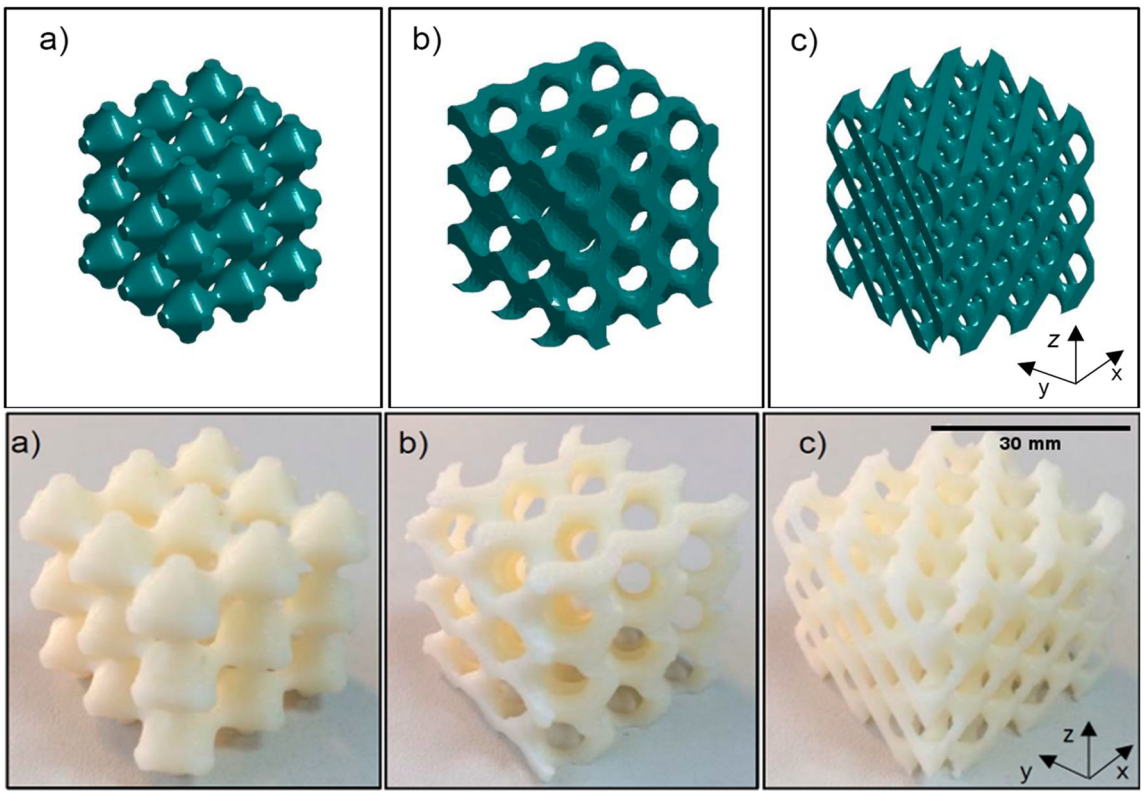

Fig. 1 CAD-planned TPMS scaffolds: **a** primitive, **b** gyroid, and **c** diamond. FDM-manufactured specimens: **a** primitive, **b** gyroid, and **c** diamond

Table 4 Support material and time for scaffold fabrication

Geometry	Support material (cm^3)	Time (h)
Primitive	8.49	2:26
Gyroid	10.91	3:36
Diamond	12.00	4:30

3 Results and discussion

Table 4 shows that significant variations were obtained for support material and manufacturing time across the TPMS scaffold types. The support material is necessary due to the downward-facing surfaces, and it is automatically generated by the AM software (CatalystEX 4.4). The primitive scaffold required the least support material and shortest manufacturing time, while the diamond scaffold required the most support material and longest manufacturing time.

The stress-strain curves from compression tests at 0° and 90° loading directions are shown in Figs. 2 and 3, respectively. The resulting maximum stress and modulus of elasticity are given in Table 5.

Comparing the stress-strain behavior of the TPMS types (see Figs. 2 and 3), it can be seen that the primitive scaffold achieves the highest stress prior to collapse for both test directions. Gyroid and diamond scaffolds show similar stress-strain behavior to one another. The maximum stress is higher at the 0° loading direction for all TPMS scaffold types. This can be explained by the mechanical anisotropy arising from the layer-by-layer manufacturing process.

The stress-strain curve observed for primitive scaffold has an initial elastic section, followed by concurrent elastic and plastic deformation up to approximately 20% strain (with the plasticity concentrated in the thin 'neck' regions) (see Figs. 8a, b), followed by structural collapse [3] (Figs. 2 and 3).

As shown in Table 5, the primitive scaffold presented a higher maximum stress in the compression test, with an average of 11.58 MPa for the 0° loading direction and 10.02 MPa, for loading at 90°. Gyroid and diamond scaffolds were around 3 times weaker than the primitive scaffold. The test direction has the greatest effect on the maximum stress for the primitive scaffold and the smallest effect for the gyroid. This can be explained by the scaffold geometry. Finally, when tested with the 90° loading direction, the built layers are parallel to the loading axis and de-bonding between layers is facilitated, promoting crack initiation and reducing the maximum stress (Fig. 4).

The complex geometry of the gyroid and diamond act as stress distributors minimizing the effect of changing load direction [18]. The gyroid performance has stable change in strength due to the internal material distribution, which is more uniform than the others [4]. Other results showed that gyroid cracks were easy to start and propagate on the upper and lower surfaces of the inclined necks [19].

The ANOVA (Table 6) for maximum stress indicates that the highest F value is for the scaffold type variable, 775.98, and the p value is ≈ 0. This indicates that the scaffold type is the most influential parameter in determining the response of the scaffolds to compressive loading. The load direction and the interaction of scaffold type × load direction have p values below 0.05 and show that all have statistically significance on maximum stress.

The graph of interactions (Fig. 5) allows the visualization of interactions through the parallelism, or not, of the lines. The greater the difference in inclination between the lines, the greater the degree of interaction [20]. For the effect of interaction between the scaffold type and load direction, it is

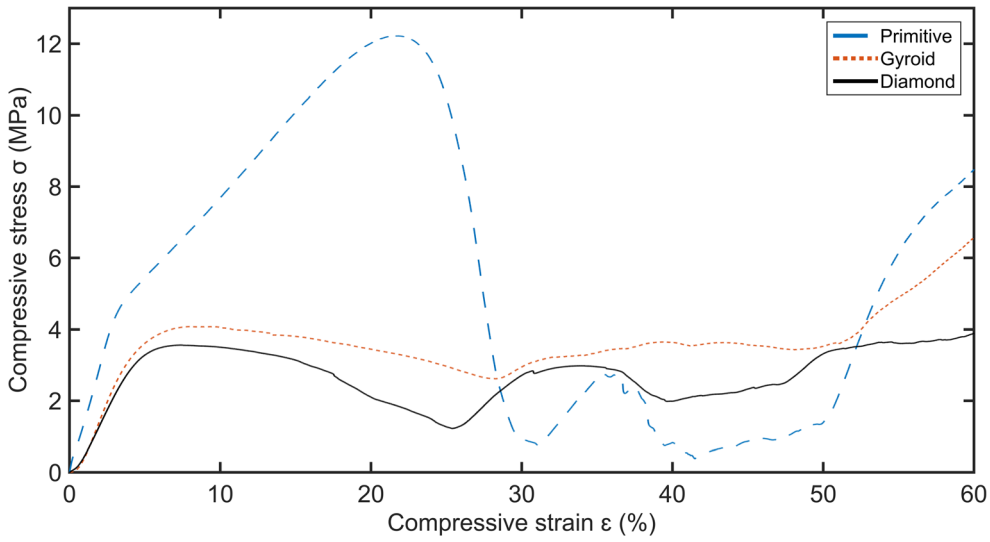

Fig. 2 Stress-strain curve for compression tests at 0° loading direction

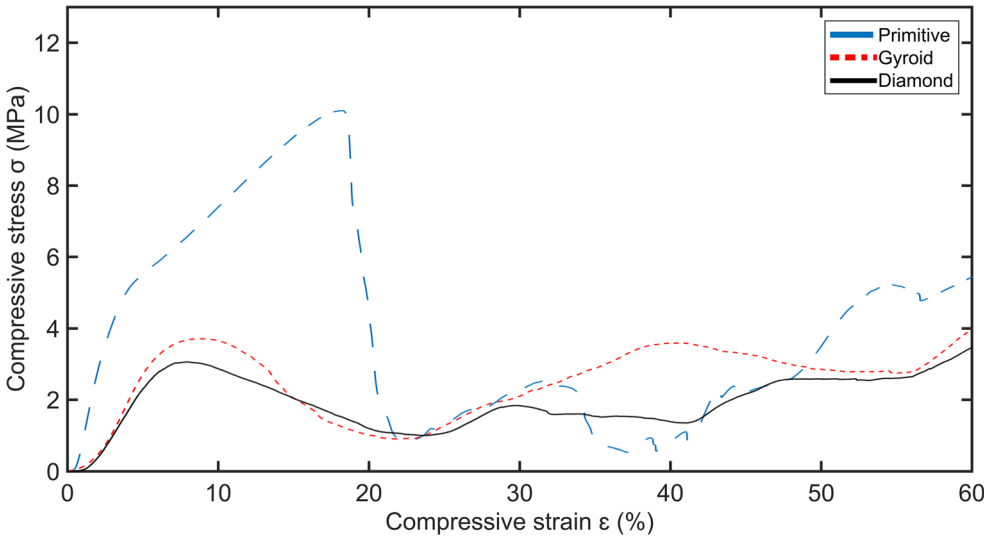

Fig. 3 Stress-strain curve for compression tests at 90° loading direction

Table 5 Compression test maximum stress and modulus of elasticity for TPMS scaffolds

Maximum stress (MPa)			Modulus of elasticity (MPa)	
Loading direction	0°	90°	0°	90°
Primitive	11.58 ± 0.82	10.02 ± 0.12	170.26 ± 12.57	173.92 ± 6.14
Gyroid	4.13 ± 0.06	4.02 ± 0.27	105.34 ± 2.15	83.15 ± 2.19
Diamond	3.59 ± 0.03	3.08 ± 0.07	85.21 ± 7.36	67.20 ± 1.73

shown that the most significant effect of interaction is for the primitive scaffold due to the decrease in maximum stress under loading at 90°. However, the interaction effects between the gyroid scaffold type and the load direction do not seem to influence the maximum stress, showing that the gyroid geometry possesses low mechanical anisotropy.

Table 5 shows that the primitive scaffold presented a higher modulus of elasticity at the 90° loading direction and gyroid

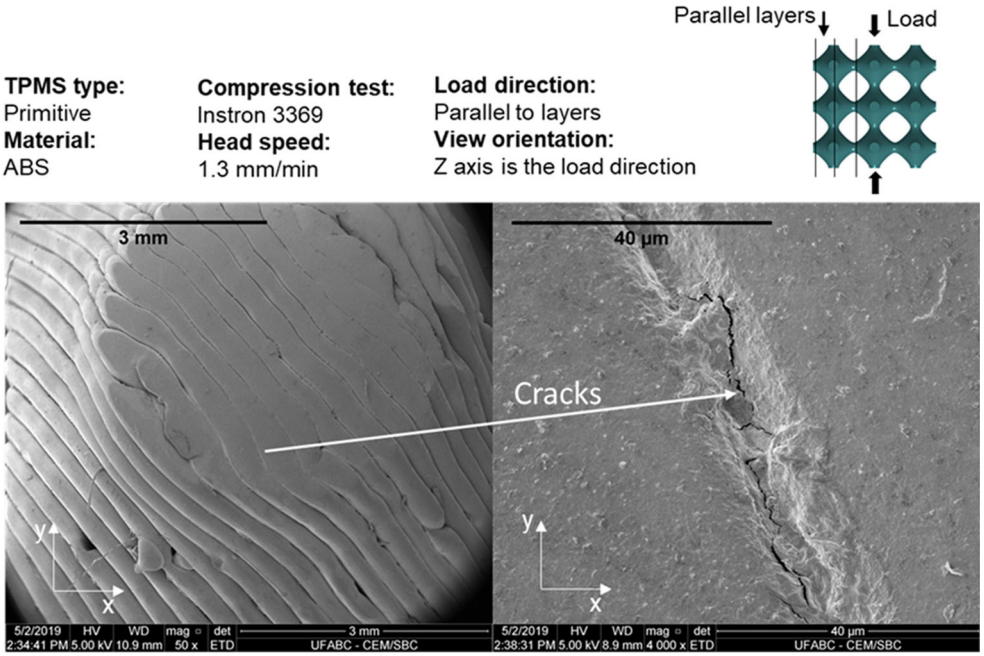

Fig. 4 Crack initiation due to debonding between layers for the primitive TPMS scaffold tested at 90°

Table 6 ANOVA for maximum stress

	df	SS (Aj.)	*F* value	*P* value
Model	5	207.118	316.56	0.000
Linear	3	205.441	523.32	0.000
Scaffold type	2	203.086	775.98	0.000
Load direction	1	2.355	18.00	0.001
Two-factor interactions	2	1.676	6.41	0.013
Scaffold type × load direction	2	1.676	6.41	0.013
Error	12	1.570		
Total	17	208.688		

Table 7 ANOVA for modulus of elasticity

	df	SS (Aj.)	*F* value	*P* value
Model	5	32,402.6	148.12	0.000
Linear	3	31,825.1	242.47	0.000
Scaffold type	2	31,157.2	356.07	0.000
Load direction	1	667.8	15.26	0.002
Two-factor interactions	2	577.5	6.60	0.012
Scaffold type × load direction	2	577.5	6.60	0.012
Error	12	525.0		
Total	17	32,927.6		

and diamond at 0°. Such behavior is related to the orientation of the FDM layers with respect to the loading direction in combination with the scaffold type. This happens because of the TPMS anisotropy [21].

The ANOVA regarding the modulus of elasticity (Table 7) shows that the scaffold type, load direction, and the interaction of scaffold type × load direction has *p* values below 0.05 and shows that all has statistical significance on modulus of elasticity.

Figure 6 shows that the interaction effect is more significant for the primitive scaffold and shows that the load direction combined with the scaffold type almost eliminates the expected anisotropic behavior of the FDM layer orientation for the modulus of elasticity. For the gyroid and diamond scaffolds, the elastic moduli obtained with a load direction of 0° were greater than those with the load direction of 90°, showing that these scaffold types possess elastic modulus anisotropy. The way the de-bonding between FDM layers occurs when loaded at 90° for diamond and gyroid scaffolds contributes to the strength reduction of these scaffold types. Although for the primitive, it seems that the necks that support the cells at 90° reduce the de-bonding layers effect, as shown in Fig. 7, the neck diameter increases in these regions and in some cases does not totally collapse like the horizontal necks.

Figure 8 shows images at the end of the compression test for scaffolds at 0° and 90° loading directions. The primitive scaffold is the only one which undergoes total structural collapse at the end of the compression test. Furthermore, primitive and gyroid scaffolds presented different fracture behaviors in different load directions, while the diamond scaffold did not. For the primitive scaffold at 0°, the fractures occur mainly at the necks parallel to the load direction. The same occurs at 90°, but for this direction, the cells of the same column stacked up (see Fig. 8b). The gyroid scaffold also had different final states in

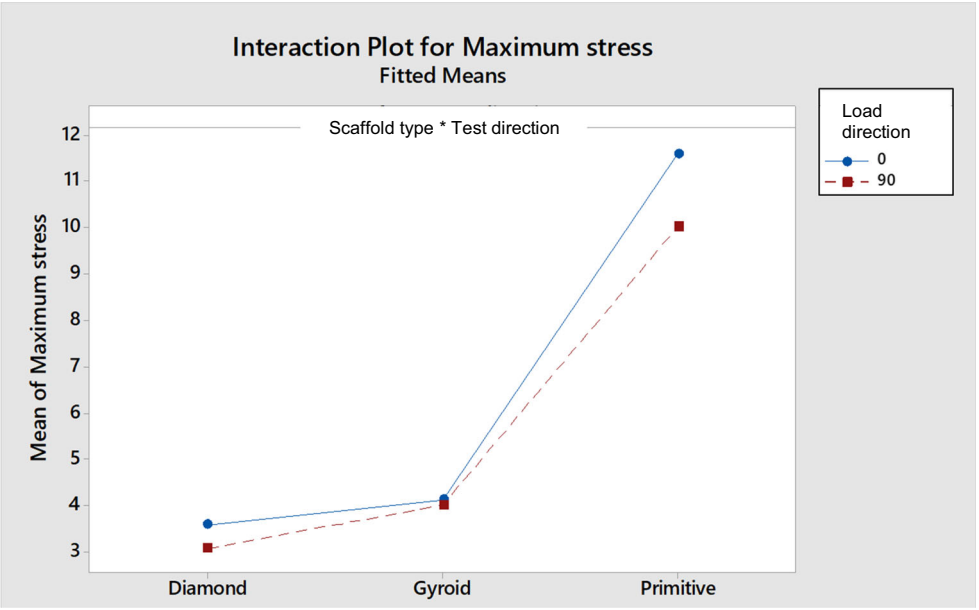

Fig. 5 Graph of the interaction effects for maximum force

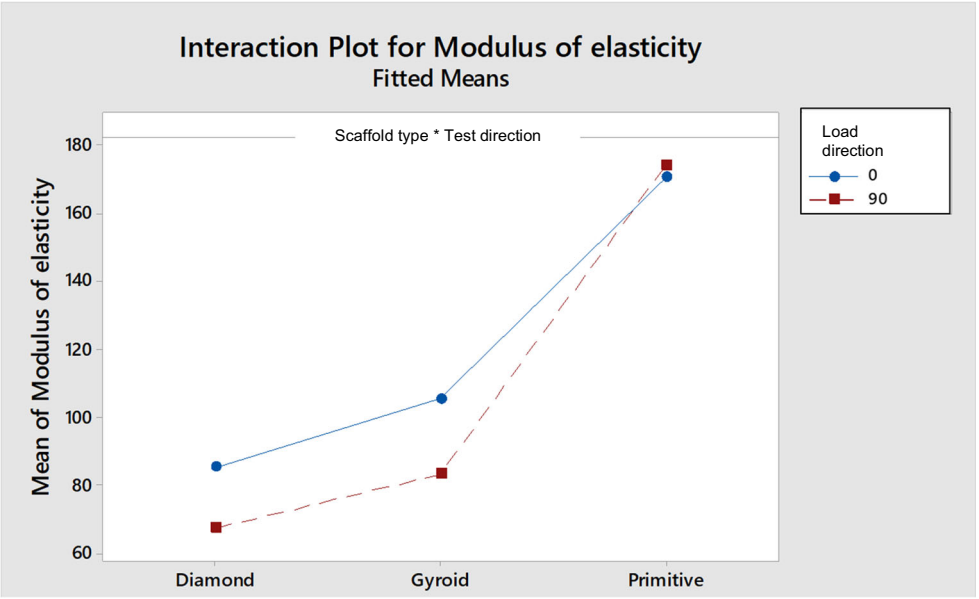

Fig. 6 Graph of the interaction effects for modulus of elasticity

different load directions: for 0° load direction, the scaffolds were compressed to a nearly square form in *x*–*y* view (34 × 32 mm), and for 90° loading, the form was elongated in *x*–*y* view (45 mm × 33 mm). This occurs when the FDM layers are aligned with the loading direction, facilitating the lateral de-bonding [6].

4 Conclusions

This work investigated the effect of the compression load direction combined with different TPMS types on the mechanical properties of scaffolds made by FDM.

The scaffold type combined with the load direction changes the maximum stress and modulus of elasticity of the scaffolds in different ways. For the maximum stress, the gyroid scaffold shows a very low difference between 0° and 90° loading directions, although for the same cell type, the modulus of elasticity has 20% difference between the load directions. The diamond scaffold shows a similar behavior and the primitive scaffold shows a low difference in maximum stress and almost the same modulus of elasticity for 0° and 90° load directions. The reported behaviors show the importance of considering the combination of the scaffold type and load direction in the design of AM scaffolds.

The primitive scaffold had the shortest manufacturing time, 2:26 h, and required the least support material, 8.49 cm^3. The gyroid and diamond scaffolds had longer manufacturing times (respectively, 48.23% and 87.61% longer than for the primitive scaffold) and required more support material (28.27% and 41.34%, respectively, greater than for the primitive scaffold).

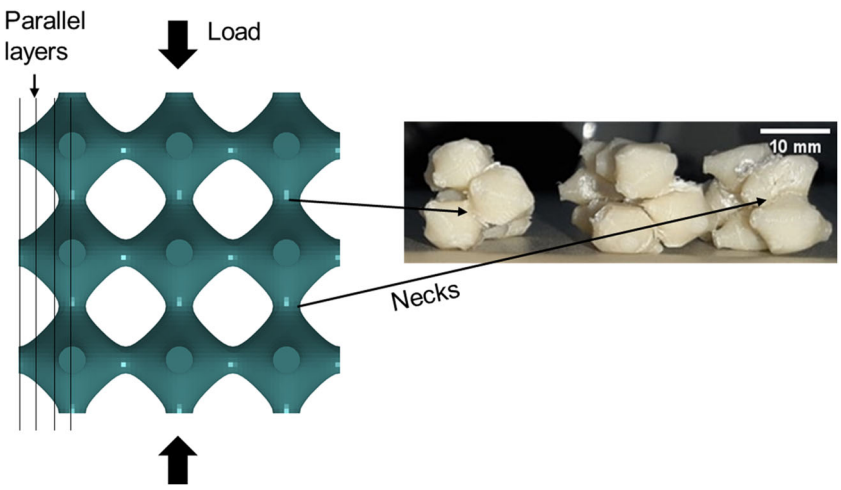

Fig. 7 Neck behavior for the primitive scaffold that support the cells in the 90° load direction

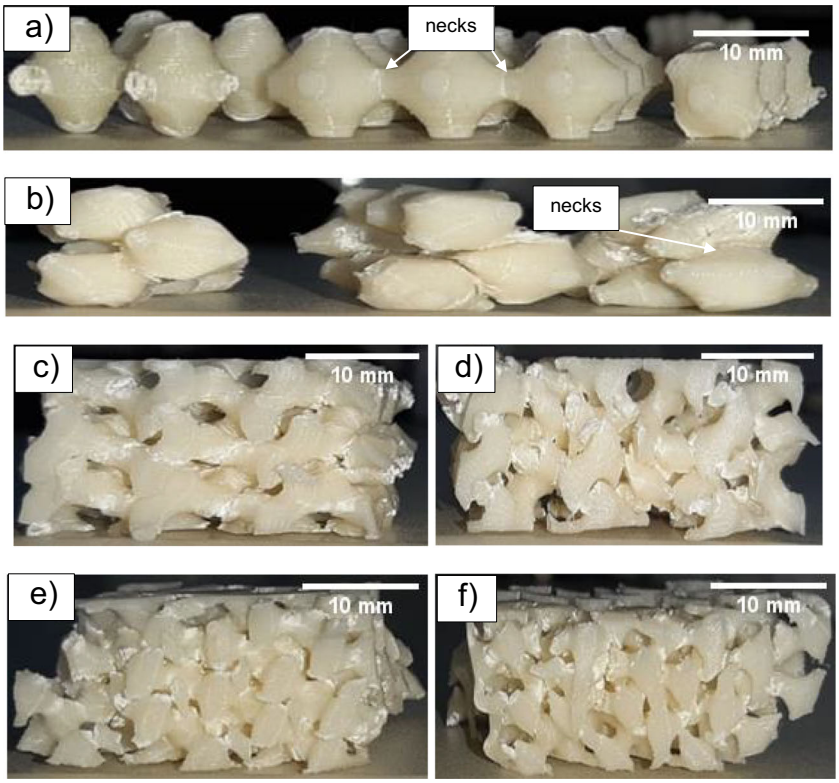

Fig. 8 End of compression tests (side view): **a** primitive scaffold at 0° (**b**) and 90°, **c** gyroid scaffold at 0° (**d**) and 90°, and **e** diamond scaffold at 0° (**f**) and 90°

The present work shows that mechanical properties are dependent on the TPMS scaffold geometry and the load direction. The FDM process has mechanical anisotropy as an intrinsic feature. However, it was shown that, by modifying scaffold geometries, the anisotropy can be increased or reduced, according to the specific requirements of the scaffold application.

Acknowledgments Special thanks are due to Henrique Lopes de Castro and Rogerio Ramos de Souza Junior. The authors are grateful to the Multiuser Central Facilities (UFABC) for the experimental support.

Funding information FAPESP, process 18/11183-2, granted scholarship for this project. Ian Maskery received fellowship funding from the University of Nottingham.

References

1. Almeida HA, Bártolo PJ (2014) Design of tissue engineering scaffolds based on hyperbolic surfaces: structural numerical evaluation. Med Eng Phys 36:1033–1040. https://doi.org/10.1016/j.medengphy.2014.05.006
2. Sreedhar N, Thomas N, Al-ketan O et al (2018) Mass transfer analysis of ultrafiltration using spacers based on triply periodic minimal surfaces: effects of spacer design, directionality and voidage. J Membr Sci 561:89–98. https://doi.org/10.1016/j.memsci.2018.05.028
3. Maskery I, Sturm L, Aremu AO et al (2018) Insights into the mechanical properties of several triply periodic minimal surface lattice structures made by polymer additive manufacturing. Polymer (Guildf) 152:62–71. https://doi.org/10.1016/j.polymer.2017.11.049
4. Zhao M, Zhang DZ, Liu F et al (2020) Mechanical and energy absorption characteristics of additively manufactured functionally graded sheet lattice structures with minimal surfaces. Int J Mech Sci 167:105262. https://doi.org/10.1016/j.ijmecsci.2019.105262
5. Lee DW, Khan KA, Abu Al-Rub RK (2017) Stiffness and yield strength of architectured foams based on the Schwarz primitive triply periodic minimal surface. Int J Plast 95:1–20. https://doi.org/10.1016/j.ijplas.2017.03.005
6. Domínguez-Rodríguez G, Ku-Herrera JJ, Hernández-Pérez A (2017) An assessment of the effect of printing orientation, density, and filler pattern on the compressive performance of 3D printed ABS structures by fuse deposition Int J Adv Manuf Technol 1–11. https://doi.org/10.1007/s00170-017-1314-x
7. Abueidda DW, Bakir M, Abu Al-Rub RK et al (2017) Mechanical properties of 3D printed polymeric cellular materials with triply periodic minimal surface architectures. Mater Des 122:255–267. https://doi.org/10.1016/j.matdes.2017.03.018
8. Sychov MM, Lebedev LA, Dyachenko S V., Nefedova LA (2018) Mechanical properties of energy-absorbing structures with triply periodic minimal surface topology Acta Astronaut 1–4. https://doi.org/10.1016/j.actaastro.2017.12.034
9. Zhang L, Feih S, Daynes S et al (2018) Energy absorption characteristics of metallic triply periodic minimal surface sheet structures under compressive loading. Addit Manuf 23:505–515. https://doi.org/10.1016/j.addma.2018.08.007
10. Restrepo S, Ocampo S, Ramírez JA et al (2017) Mechanical properties of ceramic structures based on triply periodic minimal surface (TPMS) processed by 3D printing. J Phys Conf Ser 935:012036. https://doi.org/10.1088/1742-6596/935/1/012036

11. ASTM (2013) ASTM F2971–13 Standard practice for reporting data for test specimens prepared by additive manufacturing. ASTM B Stand i:3–6. https://doi.org/10.1520/F2971-13
12. Bamiduro O, Owolabi G, Haile MA, Riddick JC (2019) The influence of load direction, microstructure, raster orientation on the quasi-static response of fused deposition modeling ABS. Rapid Prototyp J 25:462–472. https://doi.org/10.1108/RPJ-04-2018-0087
13. Khan SZ, Masood SH, Ibrahim E, Ahmad Z (2019) Compressive behaviour of neovius triply periodic minimal surface cellular structure manufactured by fused deposition modelling. Virtual Phys Prototyp 14:360–370. https://doi.org/10.1080/17452759.2019.1615750
14. Maconachie T, Tino R, Lozanovski B et al (2020) The compressive behaviour of ABS gyroid lattice structures manufactured by fused deposition modelling. Int J Adv Manuf Technol. https://doi.org/10.1007/s00170-020-05239-4
15. McCullough EJ, Yadavalli VK (2013) Surface modification of fused deposition modeling ABS to enable rapid prototyping of biomedical microdevices. J Mater Process Technol 213:947–954. https://doi.org/10.1016/j.jmatprotec.2012.12.015
16. Stratasys ABSplus P430. https://support.stratasys.com/materials/fdm-materials/absplus-p430. Accessed 2 Feb 2019
17. ASTM (2015) D 695–15 Compressive properties of rigid plastics 1. Annu B ASTM Stand i:1–8. https://doi.org/10.1520/D0695-15.2
18. Al-Ketan O, Rowshan R, Abu Al-Rub RK (2018) Topology-mechanical property relationship of 3D printed strut, skeletal, and sheet based periodic metallic cellular materials. Addit Manuf 19:167–183. https://doi.org/10.1016/j.addma.2017.12.006
19. Yang L, Yan C, Cao W et al (2019) Compression–compression fatigue behaviour of gyroid-type triply periodic minimal surface porous structures fabricated by selective laser melting. Acta Mater 181:49–66. https://doi.org/10.1016/j.actamat.2019.09.042
20. Montgomery DC (2012) Design and analysis of experiments, 8th edn. Wiley
21. Bonatti C, Mohr D (2019) Smooth-shell metamaterials of cubic symmetry: anisotropic elasticity, yield strength and specific energy absorption. Acta Mater 164:301–321. https://doi.org/10.1016/j.actamat.2018.10.034